Simulation of deformation behavior of alloy 690

Using atomistically-informed crystal plasticity model considering effect of grain boundaries

S. Chandra, M. K. Samal*

Homi Bhabha National Institute, Mumbai - 400094, India

Abstract

In this work, the deformation behavior of alloy 690 has been predicted within the framework of crystal plasticity finite element analysis by explicitly modeling finite thickness interface elements in the polycrystalline representative volume. The work involves synergistic use of material characterization, lower scale atomistic simulations and crystal plasticity analysis. The multiscale model is further used to predict the effect of grain size on material stress-strain curve and hence, the Hall-Petch effect.

Keywords: Crystal plasticity; Grain boundary effect; Atomistic simulations; alloy 690

Introduction

The prominence of grain boundaries (GBs) in governing the deformation behavior of crystalline metals and alloys has already been established [1]. During plastic deformation, the interfaces are capable of acting as dislocation nucleation sources and sinks [1]. In a real aggregate, all these traits often occur concomitantly in conjunction with bulk plasticity. Never is this truer than in the special cases of nanocrystalline or fine grained metals and alloys, which contain a relatively high density of interfaces [2]. In addition to lattice dislocations, deformation twins are also known to emit from Gbs within the abutting grains [3]. All these deformation processes occur over a range of length and time scales and are, consequently, modeled disparately within the realm of a single length or time scale tool. The linking of scale, if done at all, is through some empirical assumptions which involves murky or unmeasurable parameters for plastic deformation. It is, therefore, desired to explore new avenues for polycrystal modeling incorporating physically justified interface modeling schemes into crystal plasticity.

In view of this, we have developed a two-scale atomistic to crystal plasticity modeling approach to simulate the deformation behavior of crystalline metals. The approach involves usage of atomistic simulations to quantify the relevant activation parameters for GBs. The extracted material parameters are directly passed on to the phenomenological flow rule of crystal plasticity model at a higher length scale. At this scale, explicit grain boundaries are modeled using three dimensional finite elements and are differentiated from bulk grains by prescribing distinct flow parameters extracted from atomistic simulations. The predictive power of the adopted methodology is accessed by performing finite element simulations of uniaxial tensile behavior of alloy 690 at quasi-static strain rates at different temperatures. In addition, the traditional Hall-Petch effect [4] (increase of flow stress with reduction in grain size) is also captured. The two-scale approach explicitly includes the effect of GBs without the involvement of arbitary constants or empirical assumptions.

Material and experiments

Alloy 690 in this work is obtained in the form of plate of dimensions 200 mm × 200 mm × 5 mm. The nominal chemical composition (wt%) of the alloy is: 60.4% Ni, 29.5% Cr, 9.38% Fe, 0.44% Si, 0.34% Mn and 0.022% C. The as-received alloy is solution annealed at 11000C for 1 hr followed by water quenching. Tensile experiments at quasi-static strain rates are carried out at different temperatures of 250°C, 1500°C, 3000°C and 6000°C. After the tensile tests, microstructural characterization using scanning electron microscope is performed to determine final grain orientations and deformed texture of the material.

Fig. 1 displays a typical EBSD map showing the grain size distribution and GB character distribution in the material. The

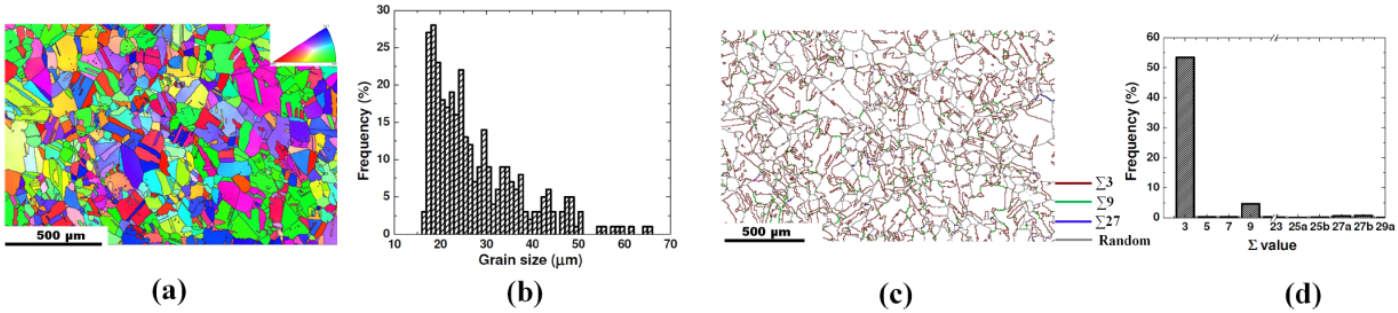

Fig. 1: (a) Initial grain orientations in alloy 690 presented by the EBSD map; (b) Initial grain size distribution; (c) GB character map and (d) distribution showing the prevalence of Σ3 boundaries in comparison to other CSL boundaries (like Σ9 or Σ27).

EBSD maps shows the prevalence of crystallographic random initial texture in the material (Fig. 1(a)). The alloy consist of equiaxed grains with an average size of 34μm (Fig.1(b)). The examination of GB character distribution map reveals that there are is a major population of Σ3 coherent twin boundaries (likely formed during annealing) and a very few higher order variants of Σ3 (like Σ9 and Σ27) boundaries (Fig. 1(c,d)). The remaining non-CSL boundaries are random boundaries (≈ 42%) which provide a connecting network to the whole EBSD map.

Fig. 2 shows that results of quasi-static tensile tests performed on alloy 690 at different temperatures. Clearly, the yield stress of the material decreases with increase in test temperature (345 MPa at 250°C, 310 MPa at 1500°C, 270 MPa at 3000°C and 220 MPa at 6000°C). A similar behavior is observed for the post yield flow stress (decrease with increasing temperature). It can, therefore, be inferred that thermally activated deformation mechanisms (dislocation motion and annihilation reactions) are the major deformation mechanisms under the investigated conditions of loading.

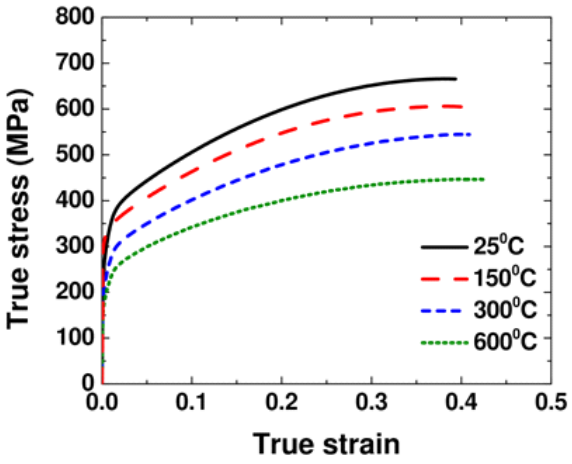

Fig. 2: Uniaxial tensile behavior of alloy 690 at different test temperatures at quasi-static strain rate.

Computational methodologies

a) Atomistics

Molecular dynamics simulations are performed using the open source code Large-scale Atomic/Molecular Massively Parallel Simulator (LAMMPS) [5] within the framework of Foiles and Hoyt [6] embedded-atom method (EAM) potential for Ni. The bicrystal models for analysis are constructed with selected orientations so as to produce Σ3 and Σ9 GBs in Ni. This is because it is observed in the EBSD scans that these two boundaries cover the major portion of the interface distribution. After checking for initial size effects and performing thermal equilibration at room temperature (300 K), the bicrystal models are subjected to uniaxial tensile loading perpendicular to the interface plane (which is oriented along y-axis). During tensile loading, microcanonical NVE ensemble is employed and velocity scaling technique is used to limit the system temperature to the desired temperature of 300 K.

Upon the application of tensile load, partial dislocation nucleation is observed in both the bicrystal models. To quantify the activation energy for this process, standard Nudged Elastic Band (NEB) calculations are performed. Specifically, these calculations take several atomic states at fixed stresses from the deformation trajectory and determines the corresponding minimum energy path at a particular value of applied stress. A total of 28 replicas are used to adequately represent the minimum energy path and the atomic states are relaxed using the fast inertial relaxation engine (FIRE) algorithm (available in LAMMPS commands) using an energy and force tolerance of 10^{-7} eV and 0.05 eV/Å, respectively, to achieve convergence.

b) Crystal plasticity simulations

The in-house crystal-plasticity based FE code CRYSP [7], developed in Reactor Safety Division, BARC, has been used in this work to perform the simulations. Within the framework of transition state theory, the embedded flow rule is given as follows [7]

$$\left|\dot{\gamma}^{\alpha}\right| = \begin{cases} 0, & if \left|\tau^{\alpha}_{eff}\right| \le 0 \\ \dot{\gamma}^{\alpha}_{0} \exp\left\{-\frac{\Delta F}{k_B T}\left[1-\left(\frac{\left|\tau^{\alpha}_{eff}\right|}{s^{\alpha}_{*}}\right)^{p}\right]^{q}\right\}, & if\ 0 < \tau^{\alpha}_{eff} < s^{\alpha}_{*} \end{cases} \quad (1)$$

Where $\dot{\gamma}^{\alpha}_{0}$ is reference slip rate, $\tau^{\alpha}_{\text{eff}}$ is the stress required for slip on slip system α, s* is thermal slip resistance, k_B is Boltzmann's constant, T is temperatures, ΔF is activation energy at zero stress and p and q are constants. These three parameters ($\Delta F, p, q$) are quantified from MD simulations for Σ3 and Σ9 GBs. The hardening rule is [7]:

$$\dot{s}^{\alpha} = \sum_{\beta} h^{\alpha\beta}\left|\dot{\gamma}^{\beta}\right|,$$

$$h^{\alpha\beta} = [q_1 + (1-q_1)\delta^{\alpha\beta}]h_0^{\beta}\left|1-\frac{s^{\beta}}{s_s^{\beta}}\right|^{r} \quad (2)$$

where $\delta^{\alpha\beta}$ is the Kronecker delta, $h^{\alpha\beta}$ is the latent hardening matrix which takes care of self as well as latent hardening of slip systems, q_1 is the latent hardening parameter, h_0 is hardening parameter, s_s is saturation slip resistance and r is the hardening exponent [7].

The Representative Volume Element (RVE) (500 μm cube consisting of 216 grains and 29,791 hexahedral finite elements with reduced integration) for alloy 690 is created using three dimensional Voronoi tessellation method. The experimentally observed initial grain size distribution (Fig. 1) and random grain orientations (using MTEX [8]) are superimposed on the RVE of alloy 690. To model finite thickness GBs, which basically represents a GB affected region (GBAR), a Java based program is developed. The program parses the input mesh file containing nodal coordinates and element-node relationship and tags the two elements as boundary elements if they share 4 nodes and belong to different grains. Thus, the GBAR in our work (by the choice of uniform meshing of the RVE) is two element thick (one element in each abutting grain). It may be noted that although the interface elements carry the

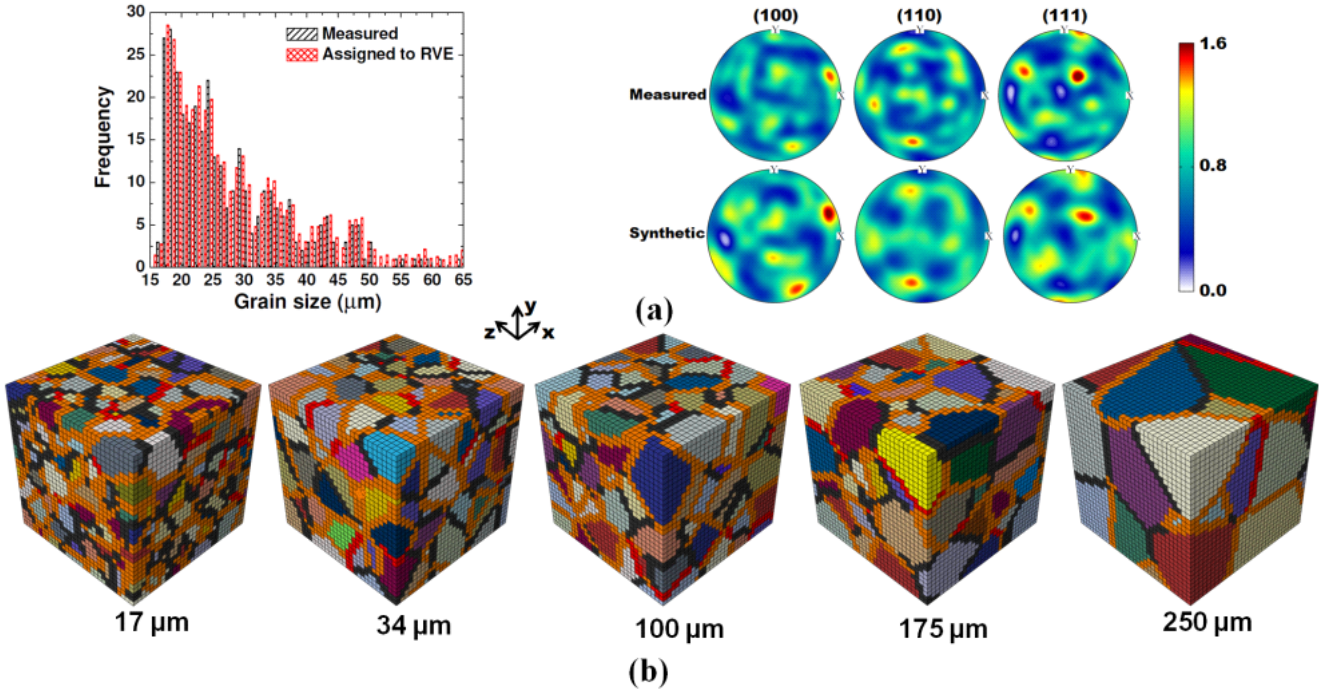

Fig. 3: (a) Initial grain orientations and texture assigned to alloy 690; (b) RVEs of different grain sizes showing the interface elements as mentioned in the text.

initial grain orientations of the abutting grains themselves, use of explicit finite elements representing the interface affected region allows us to assign distinct constitutive parameters of the crystal plasticity model to these elements.

Out of the total of 1080 interfaces present in the RVE of mean grain size 34 μm 53.4% (577 boundaries) are classified as Σ3 and 4.7% (51 boundaries) are classified as Σ9 boundaries (ignoring Σ27 boundaries). The remaining (452) boundaries are random boundaries. Similar interface character assignment is done for other volume elements of different grain sizes, which are shown in this figure, orange, red and gray color finite elements represent, respectively, Σ3, Σ9 and random interface affected regions. Uniaxial tension is applied on the RVE after imposing sufficient constraints to prevent rigid body motion.

Results and discussion

a) Atomistic simulations

NEB calculations are performed at different values of applied stress in MD simulations and the obtained results are shown in Fig. The points in figure are NEB results and solid lines are fit to the following characteristic equation, which forms the basis of flow rule of the adopted CP model:

$$\Delta G = \Delta F\left[1-\left(\frac{\sigma}{\sigma_c}\right)^p\right]^q \qquad (3)$$

The aforementioned fit allows us to quantify $\Delta F, p, q$ for both the GBs for use in CP simulations. The atomistically determined parameters using the NEB calculations are mentioned in Table 1.

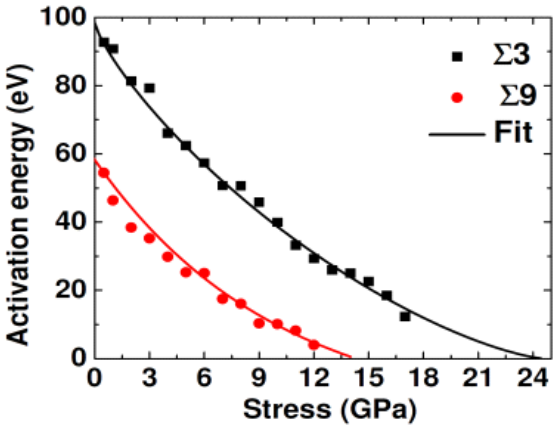

Fig. 4: Uniaxial tensile behavior of alloy 690 at different test temperatures at quasi-static strain rate.

Table 1: $\Delta F, p, q$ for Σ3 and Σ9 GBs determined from NEB calculations.

Boundary	ΔF (eV)	p	q
Σ 3	98.38	0.798	1.397
Σ 9	56.74	0.585	1.720

b) CP simulations

The CP model parameters for bulk grains of alloy 690 as well as GBs (from atomistic simulations) are mentioned in Table 2. Using these parameters, Fig. 5(a,b) displays a comparison of the experimental and CP simulation results of tensile deformation of the material at various test temperatures in the form of mechanical stress-strain curves and bulk texture evolution after deformation. A close match with the experimental data corroborates the capability of the adopted two-scale methodology in predicting the mechanical behavior of the material under the investigated conditions of loading.

Table 2: Material parameters used to simulate the mechanical behavior of alloy 690 using CP

Elastic stiffness	Constitutive parameters	Grains	Σ3 GBs	Σ9 GBs	Random GBs
C_{11} = 277 GPa	(x $10^{6}s^{-1}$)	6.0	6.0	6.0	6.0
C_{12} = 118 GPa	ΔF (J)	7.0×10^{-19}	15.74×10^{-18}	9.08×10^{-18}	1.75×10^{-19}
C_{44} = 79 GPa	p	0.80	0.798	0.585	0.683
	q	1.45	1.397	1.720	1.241
	q_1	1.4	1.4	1.4	1.4
	r	2.5	2.5	2.5	2.5
	s_0 (MPa)	142.0	1.0	1.0	1.0
	h_0 (MPa)	889.0	889.0	889.0	889.0
	s_s (Mpa)	406.0	406.0	406.0	406.0

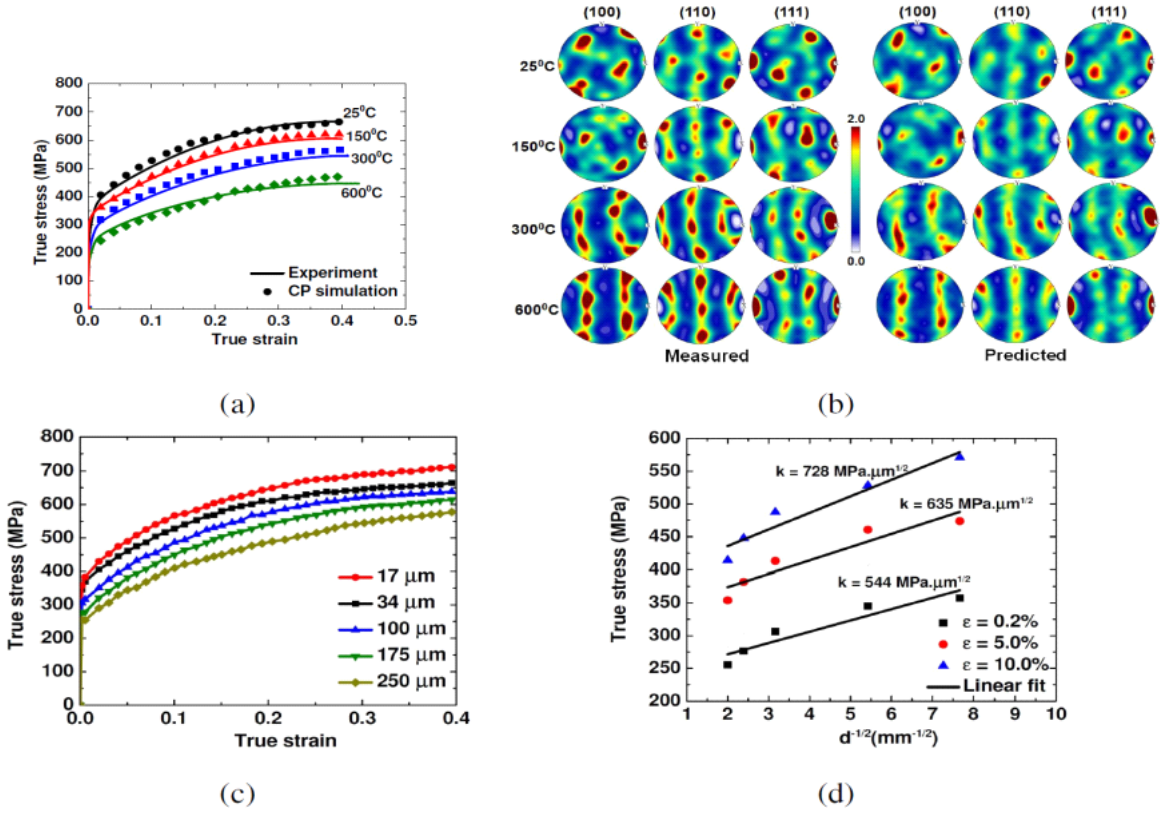

Fig. 5: Predictions of (a) tensile stress-strain curves, (b) textures at different temperatures, (c) stress-strain curves with grain sizes and (d) flow stress with grain size obtained from CP simulations of alloy 690.

In addition, the dependence of flow stress on grain size and the resulting linear HP slope [4] is also appreciably captured by the adopted methodology, as is depicted in (Fig.5 (c,d) Several interpretations can be envisioned for such observed behavior. For instance, one can cite the examples of popular pile-up models of dislocations, which were the original mechanisms used to interpret the HP effect. Within the framework of gradient plasticity theory [9], the strain incompatibility type models explain the existence of HP effect due to the existence of geometrically necessary dislocations. Another class of models relate the polycrystal to a composite [10], where the bulk grains and GBs are of different strength. The presence of relatively hard GB regions in the polycrystal leads to an increase in stress with reduction in grain size.

The dependence of flow stress of alloy 690 on grain size in this work can be directly related to the amount of GB material present in the RVE of the alloy. As can be seen from Table 2, behavior of elements corresponding to Σ3 and Σ9 GBs in our computational formulation is relatively hard (higher ΔF) ascompared to that of the bulk grains. Therefore, as the grain size reduces, the relative amount of hard material increases. Thus, smaller grain size models have a higher volume fraction of the GB elements, and thus harder material. This is the primary mechanism responsible for capturing the increase in flow stress with decrease in grain size in our CP simulations of alloy 690. In addition, the presence of GBAR may alter the dislocation mean free path. Therefore, it is clear from the aforementioned simulations that our methodology is able to predict the grain size dependence of flow stress in alloy 690 under the given conditions of loading.

Conclusions

The material stress-strain curve of alloy 690, its temperature-dependence and the influence of grain size on stress-strain curve, have been captured through a new two-scale material modeling technique, where the parameters have been transferred from atomistic scale to the crystal-plasticity length scale. Through the use of explicit interface elements for the grain boundaries, the polycrystalline response has been simulated satisfactorily through the use of FE-based in-house code CRYSP. It is envisioned that the approach can be generalized and pushed forward to include many other thermally activated GB-related deformation mechanisms. Complemented by electron microscopy, the interface makeup of the material can be determined and modeled using a RVE, thereby making this methodology very simple and convenient for persual.

Corresponding Author*

Dr. M.K. Samal (mksamal@barc.gov.in)

References

[1] J. P. Hirth, The influence of grain boundaries on mechanical properties, *Metall. Trans.* **3** (1972) 3047–3067.

[2] S. N. Naik, S. M. Walley, The Hall-Petch and inverse Hall-Petch relations and the hardness of nanocrystalline metals, *J. Mater. Sci.* **55** (2020) 2661–2681.

[3] Q. Li, L. Wang, J. Teng, X. Pang, X. Han, J. Zou, In-situ observation of cooperative grain boundary sliding and migration in the nano-twinned nanocrystalline-Au thin-films, *Scr. Mater.* **180** (2020) 97 – 102.

[4] E. Hall, *Proc. Phys. Soc.* Lond. **B 64** (1951) 747–753.

[5] S. Plimpton, Fast parallel algorithms for short-range molecular dynamics, *J. Comput. Phys.* **117** (1995) 1–19.

[6] S. M. Foiles, J. J. Hoyt, Computation of grain boundary stiffness and mobility from boundary fluctuations, *Acta Mater.* **54** (2006) 3351–3357.

[7] M. K. Samal, Development of a model for simulation of micro-twin and corresponding asymmetry in high temperature deformation behavior of nickel-based superalloy single crystals using crystal plasticity based framework, *J. Mech. Eng. Sci.* **231** (2017) 2621–2635.

[8] R. Hielscher, H. Schaeben, A novel pole figure inversion method: Specification of the MTEX algorithm, *J. Appl. Cryst.* **41** (2008) 1024–1037.

[9] J. Aldazabal, J. G. Sevillano, Hall–Petch behaviour induced by plastic strain gradients, *Mater. Sci. Eng.*, **A 365** (2004) 186–190.

[10] D. Benson, H. Fu, M. Meyers, On the effect of grain size on yield stress: extension into nanocrystalline domain, *Mater. Sci. Eng.* **A 319** (2001) 854–861.